Phase separation in $Cu_{90}Co_{10}$ high-magnetoresistance materials

M. G. M. Miranda,[1,2] E. Estévez-Rams,[2,3] G. Martínez,[1] and M. N. Baibich[1]
[1]*Instituto de Física, UFRGS, Caixa Postal 15051, 91501-970 Porto Alegre, RS, Brazil*
[2]*Centro de Microscopia Eletrônica, UFRGS, Caixa Postal 15051, 91501-970 Porto Alegre, RS, Brazil*
[3]*Universidad de la Habana, IMRE, C.P. 10400, C. Habana, Cuba*
(Received 2 May 2002; revised manuscript received 18 March 2003; published 30 July 2003)

The relation between giant magnetoresistance (GMR) and phase separated nanostructures in $Cu_{90}Co_{10}$ is studied using magnetotransport measurements together with transmission electron microscopy and *x*-ray microanalysis. The samples were melt-spun ribbons isochronally annealed up to 873 K, and all show in their grains a homogeneous spinodal decomposition characterized by long parallel Co-excess stripes. These stripes have 40-nm modulation periods and develop along the crystalline directions of each grain. Different anneals do not change appreciably the observed microstructures, while the magnetoresistance is initially enhanced by a factor of 2, followed by a 35% drop above 823 K. The latter coincides with the observation of a secondary lamellar decomposition of 4 nm modulation length. We propose that the GMR effects in CuCo alloys originate from these nanoscopic modulations of the constituents induced by nonequilibrium processes.

DOI: 10.1103/PhysRevB.68.014434 PACS number(s): 75.47.De, 45.70.Qj, 64.70.Kb, 81.40.Rs

I. INTRODUCTION

The discovery of giant magnetoresistance (GMR) in magnetic multilayers[1,2] opened new areas in magnetism and magnetic materials research at the nanoscopic scale. Later on, magnetic granular systems were found to have similar effects[3,4] and $Cu_{1-x}Co_x$ was one of the first compounds to be investigated for GMR effects. Initially, this alloy was assumed to be a standard granular system, but we show in the following that this is not quite the case, as other microstructures are involved.

Magnetic granular alloys are conventionally conceived as being composed basically of magnetic granules (nanoclusters) embedded in a nonmagnetic metallic matrix. A number of phenomenological models to explain GMR in granular materials consider these granules, resulting from segregation processes, as the main source for electronic spin-selective scattering either accounting for possible interactions between the (saturated) magnetic granules[5] or analyzing its size or moment distribution.[6] Although relatively successful in describing true granulars, such as AgCo and many others,[4] these models were not able to fully explain all the observed results in CuCo alloys, such as the high-field saturation of the magnetoresistance[7] or ferromagnetic resonance effects.[8] Recent studies,[9] testing the interplay of granular size dispersion and dipolar magnetostatic interactions in the GMR properties of CuCo suggest that in spite of having a reasonable agreement between model and experimental results, a bona-fide description of the microscopic structures is strongly needed. More recently, Vergara and Madurga[10] studying the effect of isothermal heat treatments in CuCo ribbons arrived basically at the same conclusion. Many other works about these melt-spun ribbons could be mentioned, in particular, the findings of Panissod *et al.*,[11] which show the presence of two magnetic components for a hypothetical distribution of grain sizes, or those of López *et al.*[12] in showing the need for a double magnetic density for the Co grains in lower concentration alloys.

In the search for a reliable description at the nanoscopic scale, many models for GMR in granular alloy systems assume, as we said, dispersed magnetic granules within the structural grains. For the CuCo system, the assumption is to have superparamagnetic Co nanoclusters embedded in a Cu-rich conductive matrix. The results of different magnetic measurements (mainly magnetization data) are usually interpreted to obtain the distribution of moments (or sizes) of these hypothetical magnetic granules. These measurements are, in fact, the result of a statistical average over different local configurations, and should only be safely applied if the existence of a nonpercolative granular formation is confirmed. Notwithstanding, on account of the averaging characteristic of the magnetic results, other possible morphological configurations could have their results reasonably explained by spherical granules, thus blurring the real sources for spin-selective electron scattering in these materials. Special attention should be given in this case to self-organized structures at the nanoscopic scale coming from interactions between the constituents.

As a matter of fact, CuCo is not a simple granular material, for it is well known to exhibit a large miscibility gap[13] with a wide metastable region. This has made it for decades a good example for spinodal decomposition,[14] as well as for nucleation and growth studies at the late stages of the process.[15] Lately, this pair of transition metals has also been used to evaluate observation techniques for precipitates in transmission electron microscopy (TEM),[16] since these elements are rather difficult to distinguish by standard methods on account of the very similar atomic numbers and bulk lattice parameters (in the fcc lattice). In spite of the drawbacks, a couple of works did get direct visualization of spinodal decomposition in CuCo alloys.[17,18]

Spinodal decomposition is understood as a form of segregation that takes place in some nonequilibrium alloys, where the concentration of the solute varies almost sinusoidally within a few hundred lattice parameters along certain crystalline directions. Precipitates of the solute, on the other hand, can ultimately be induced by thermal activation starting from spinodally decomposed regions, as observed in sev-

 ©2003 The American Physical Society

eral immiscible materials.[19] It is relevant to point out that the mere presence of precipitates cannot, by itself, tell whether they have been formed from spinodal decomposition or by nucleation and growth processes. Although many works on GMR materials deal with true granular compounds, in the sense that those alloys do not undergo spinodal decomposition,[4] a number of so-called granulars does present this phase separation, making the analysis of GMR properties more difficult because of the domain-wall associated magnetization processes that have to be considered.[12] In some cases, the lamellar decomposition was even suggested to be responsible for producing GMR out of two ferromagnetic phases.[20]

Because of the above-mentioned difficulties in observation at the nanoscopic scale and the complex microstructures we see in these materials, the link between microstructural changes and magnetotransport properties is not fully understood yet. In order to shed light on the evolution of the microstructures with the anneals and correlate it to the resistivity behavior, as well as to the appearance of GMR and its changes, we have done a systematic study of the behavior of $Cu_{90\mp5}Co_{10\pm5}$ melt-spun ribbons, based on an isochronous thermal procedure to be described below. Here, we concentrate on the 10% Co content, which is known to be in the unstable region of the phase diagram[13] of the CuCo system that forces the appearance of spinodal decomposition.[17] It also shows a sizeable GMR from the as-spun state onward, as our previous work demonstrated.[21]

In this paper, we show that the difficulties to understand GMR effects in CuCo alloys are indeed related to the lack of an accurate determination of the actual microstructures. As we shall see in the following, the resulting microstructures in these materials are initially more complex than a simple granular alloy that evolves to the limit of coalescence. The as-made (melt-spun) CuCo samples are described by randomly oriented structural fcc grains of 500–3000 nm size, each of which has already developed a lamellar spinodally decomposed phase, with a fixed period of 35–45 nm. Thermal anneals first enhance the MR (doubling its value), which is then followed by a marked decrease above 823 K. The latter might be the result of taking the system into an irreversible region at high temperatures, where a secondary finer ($\sim$4 nm) lamellar spinodal decomposition also appears. Since no apparent change in the modulation length of the lamellar structure is observed below 823 K, we propose that the increasing amplitude of the spinodal oscillations with the anneals is the key to understand the MR enhancement. As the segregated material is Co (or a Co-rich CoCu alloy, dense enough to be magnetic), this would form smooth interfaces where spin-selective electron scattering could take place, thus favoring the enhancement of MR with the amount of segregated Co. On the other hand, the subsequent decrease of MR above 823 K should be associated with the smaller period lamellae which appear at higher annealing temperatures. Such a reduction in the modulation length might induce a decoupling of the effective Rudermann-Kittel-Kasuya-Yosida interaction (or its equivalent) between Co-rich regions, disfavoring MR in this case.

II. EXPERIMENTAL

The CuCo ribbons were produced at the Istituto di Fisica, Torino, Italy, by standard planar flow casting at nearly 35 m/s in a controlled Ar atmosphere, with high quenching rates of $\approx 5\times10^5$ K/s. Subsequent characterization of the samples, the magnetotransport analysis, TEM imaging, and energy dispersive spectroscopy (EDS) microanalysis were done at the Instituto de Física and Centro de Microscopia Eletrônica, UFRGS, Porto Alegre, Brazil, respectively.

We have measured *in situ* the resistivity of the samples as a function of temperature with a home-made, low-frequency, four-probe ac detection bridge,[22] during isochronous anneals for different final interruption temperatures T_f, from 494 to 873 K, reproducing the GMR results described in our previous work.[21]

Each sample was thermally treated only once to follow the effect of the anneals. The anneals took place in a specially made lamp furnace with high precision temperature and heating rate controls. Each annealing procedure consisted in the same controlled heating process, always at the same constant (isochronal) heating rate of 9.8 K/min until the final annealing temperature was reached. At this temperature T_f, heating was interrupted and the cooling process started immediately. The cooling cycle can be described by a nearly constant slope of around -2.5 K/s. This rate is sufficient to ensure the quenching of the thermodynamic state attained at T_f. Subsequently, the magnetization and magnetoresistance were measured: the magnetization in a dc SQUID magnetometer[23] in magnetic fields up to 5 T at three different temperatures, 4.2, 20, and 300 K, and the magnetoresistance in fields up to 6.5 T, at 4.2 and 300 K. With this procedure, we follow the magnetotransport changes with the anneals, and relate them to the evolution of the microstructures.

Images of TEM and x-ray microanalysis have been used to characterize the microstructures for each step of the annealing process. For this analysis, the samples were prepared by the tripod polisher technique and ion milling, and observed in a 200-kV-JEM 2010 analytical microscope equipped with an energy dispersive NORAN-Pioneer microanalysis system (EDS) using a Si detector. We prepared and analyzed with TEM and EDS at least three different samples for each kind of heat treatment (''as-made'' and the various T_f isochronous anneals).

III. RESULTS AND DISCUSSION

A. Magnetotransport properties

We first focus on the magnetotransport properties of our samples. Since we measure the resistivity as a function of applied field and temperature, we will write it as $\rho=\rho(H,T)$, denoting field induced changes as $\Delta\rho_H=\rho(H,T)-\rho(0,T)$ and thermal changes as $\Delta\rho_T=\rho(0,T)-\rho(0,300)$. When not specified, the following notation is also used: $\rho(T)=\rho(0,T)$. The resistivity of the samples before annealing was found to be $\approx 70\ n\Omega$ m.

Figure 1 displays the normalized *in situ* resistivity changes $\Delta\rho_T/\rho(300\ \mathrm{K})$ as a function of temperature. This

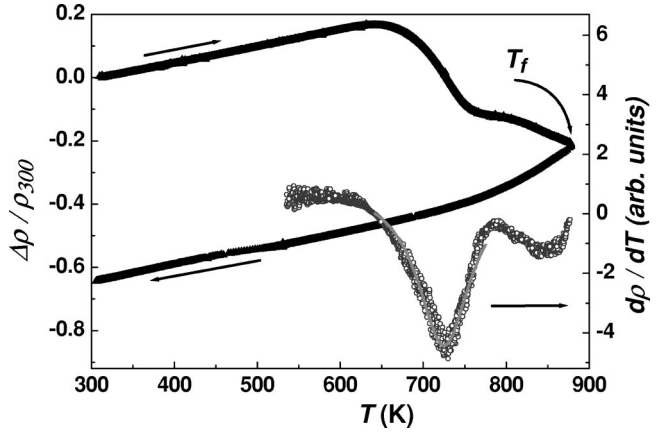

FIG. 1. Normalized thermal changes of the *in situ* resistivity, $\Delta\rho_T/\rho(300)$ (left-hand side), and its derivative $d\rho/dT$ (right-hand side), as a function of temperature, for $Cu_{90}Co_{10}$ samples. A linear behavior in $\Delta\rho_T/\rho(300)$ is observed below 650 K and a clear irreversible decrease above it, as seen from the return cooling path after annealing up to T_f. The irreversible ''nose'' above 650 K is a general feature in these alloys. Also, a clear minimum at 723 K occurs for $d\rho/dT$ during the anneal for all $Cu_{90\pm5}$ $Co_{10\pm5}$ samples.

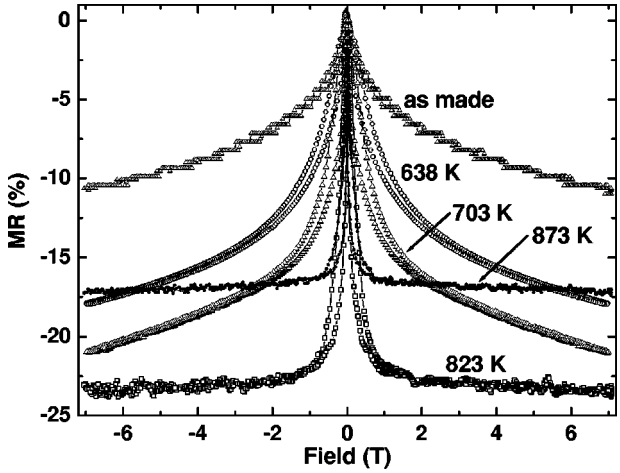

FIG. 2. Magnetoresistance (MR) versus field of different annealed $Cu_{90}Co_{10}$ samples measured at a low temperature $T=4.2$ K. Indicated temperatures are the final annealing temperatures T_f of isochronous anneals for each sample. Some hysteresis is observed on each curve. Note that the largest saturation value of MR occurs at $T_f=823$ K, but then drops abruptly for higher $T_f=873$ K.

quantity increases linearly up to 650 K, above which it has an irreversible decrease up to $T_f=873$ K, the largest final annealing temperature we have studied. As previously shown by some of us,[24] each return cooling path, as the one indicated in the picture, is fully retraceable after we reinitiate the annealing process (which is, however, *not* discussed in this work, where the samples were treated only once, at a constant heating rate up to T_f and then cooled down to room temperature). On the right-hand scale of Fig. 1, we have plotted the derivative of the resistivity for the heating process, $d\rho/dT$, which shows a clear minimum around 723 K, followed by changes in slope above it. The very same behavior is seen in that temperature range for the other Co concentrations of $Cu_{1-x}Co_x$ studied by us ($x=5\%$ and 15%), with a minimum in $d\rho/dT$ at nearly the same temperature.[27] These other concentrations correspond to ribbons produced with the same quenching parameters reported here for $x=10\%$ and belong to the same instability region of the phase diagram. This leads us to believe that the event marked at this particular temperature (723 K) depends essentially on the chemical species involved. Such an observation is a further evidence that ''chemical repulsion,'' one of the requirements for spinodal decomposition, is indeed present.

Figure 2 shows the $MR=\Delta\rho_H/\rho(T)$ versus applied field of the annealed $Cu_{90}Co_{10}$ samples measured at $T=4.2$ K, for different final annealing temperatures T_f, as indicated. Some hysteresis is observed in our results, which is consistent with the literature.[25,10] The hysteretic state at low temperatures is sometimes associated with a blocking process,[26] taken as an evidence of a superparamagnetic state[10] of these alloys, but this has to be reconsidered on account of our observations in this work. Figure 2 also shows that the saturation value of MR grows steadily up to $T_f=823$ K, then drops for the next final annealing temperature $T_f=873$ K. From a previous study[21] in $Cu_{1-x}Co_x$ alloys we know that as T_f is increased the apparent saturation field (from hysteresis loops) reduces continuously, indicating that the degree of ferromagnetic character increases with the anneals. Our present study is fully consistent with this observation. In Fig. 2, this translates into the deviation from the parabolic behavior of MR and, consequently, smaller saturation fields for higher T_f.

Figure 3(a) shows the absolute values of the saturation MR, taken at 6.5 T, as a function of the final annealing temperatures T_f, measured at $T=4.2$ K and 300 K. In either case, we see that the behavior of the magnetoresistance is basically the same: its saturation value grows continuously, roughly doubling upon reaching $T_f=823$ K, and then droping abruptly (by nearly 35%) for the next $T_f=873$ K. The largest MR ($\sim$23.5% for $T=4.2$ K) appears close to the point where the negative slope in the resistivity increases again in magnitude ($\sim$823 K). This point is in the upper part of the irreversible region starting at 650 K, as depicted in Fig. 1, beyond which the results do not cyclically reproduce the values for the resistivity.

Figures 3(b) and 3(c) show, respectively, the values for $\Delta\rho_T/\rho(300)$ and magnetization M, after annealing, at room temperature, as a function of T_f. Note that while $\Delta\rho_T/\rho(300)$ decreases continuously from $T_f=650$–823 K, the magnetization and the magnetoresistance increase in this range. The fact that the magnetization grows is consistent with an enhanced degree of ferromagnetic character, as measured from the reduction of the saturation field from hysteresis loops.[7] On the other hand, a scrutiny of Fig. 1 indicates that a number of different segregation processes are taking place while the annealing temperature is raised above 650 K, as they are associated to different slopes of the resistivity[21] during the anneals. Such processes are linked to structural changes of many different origin such as all kinds of migration, diffusion, phase separation, dislocations, stress relief. As the changes involving magnetic species may have a crucial effect on the magnetic behavior of the treated samples,

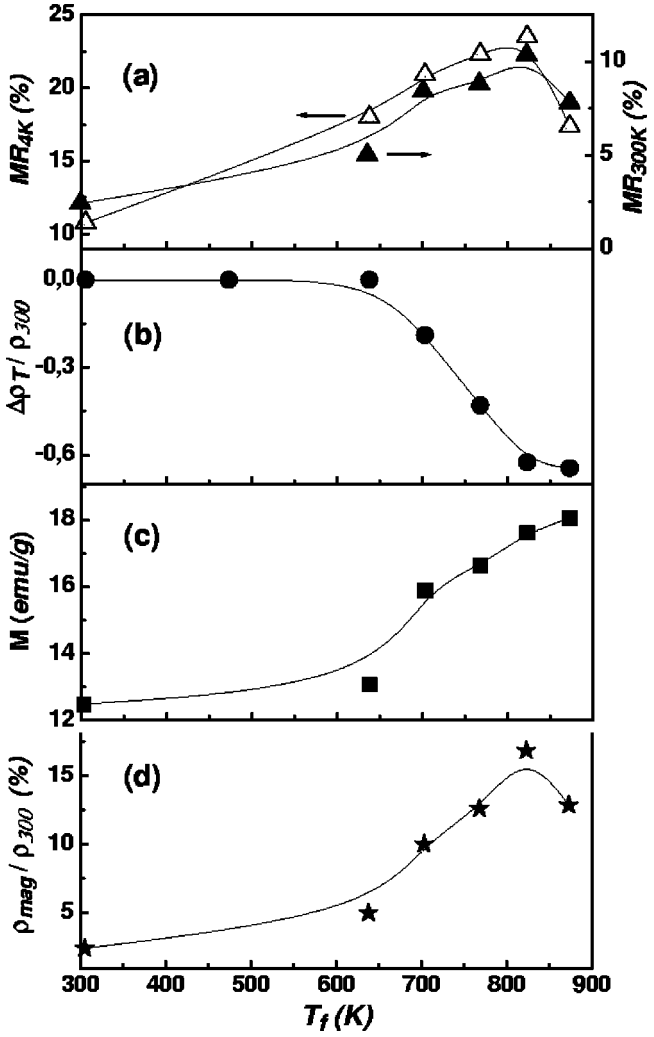

FIG. 3. (a) Absolute values of the saturation magnetoresistance (MR) (at 6.5 T), as a function of T_f, measured at low (4.2 K) and at room temperatures (300 K); (b) Values of $\Delta\rho_T/\rho(300)$, after annealing, as a function of T_f; (c) Magnetization M at 5 T, as a function of T_f; and (d) Normalized ''magnetic resistivity'' component ρ_{mag}/ρ_{300}, as a function of T_f. All lines are just guides for the eye.

we believe that the microstructural changes responsible for the changes in the resistivity are also responsible for the magnetic changes that determine the electronic scattering, and as a result, the behavior of the magnetoresistance.

The magnetoresistance can be described schematically as

$$\mathrm{MR}=\frac{\Delta\rho_H}{\rho(T)}=\frac{\rho(H,T)-\rho(0,T)}{\rho(0,T)}, \tag{1}$$

that is, the ratio between the resistive changes arising from magnetic scattering and the total (zero field) resistivity. This means that the enhanced MR observed after annealing might come from reducing the residual resistivity (by stress relief, for example), from an increasing magnetic contribution, or even from both processes at once.

Because of the irreversibility region in Fig. 1, the sample resistivity before and after the annealing differ. We shall label them $\rho_0(T)$ and $\rho_{T_f}(T)$, respectively. The effect of the annealing is represented, at room temperature, through the expression

$$\left.\frac{\Delta\rho_T}{\rho_0}\right|_{\text{annealing}}=\frac{\rho_{T_f}(300\ \mathrm{K})-\rho_0(300\ \mathrm{K})}{\rho_0(300\ \mathrm{K})}, \tag{2}$$

which has been plotted in Fig. 3(b). Now, extending Mathiessen's rule, we may extract the magnetic-field dependent part of the resistivity as follows:

$$\rho_{T_f}(H,T)=\rho_0(T)+\rho_{\mathrm{mag}}(H,T). \tag{3}$$

Assuming the property $\rho_{\mathrm{mag}}(0,T)=0$, then $\rho_0(300\ \mathrm{K})=\rho(0{,}300\ \mathrm{K})$ is the sample resistivity before annealing. At room temperature, we have

$$\mathrm{MR}(300\ \mathrm{K})=\frac{\rho_{\mathrm{mag}}(H_S,300\ \mathrm{K})}{\rho_{T_f}(300\ \mathrm{K})}, \tag{4}$$

where H_S is the saturation field. After simple algebra, we arrive at

$$\frac{\rho_{\mathrm{mag}}(H_S,300\ \mathrm{K})}{\rho_0(300\ \mathrm{K})}=\mathrm{MR}(300\ \mathrm{K})\left(1+\frac{\Delta\rho_T}{\rho_0}\right). \tag{5}$$

The result of this procedure is shown in Fig. 3(d), where a substantial change in trend is seen above 638 K, with a large maximum at the 823 K threshold. It seems rather clear from this simple analysis that the increase, followed by a sharp drop of MR for T_f above 823 K, is mainly associated with a magnetic effect in the irreversible region which deserves further investigation.

B. Microstructures

TEM results have revealed that all observed $Cu_{90}Co_{10}$ samples, for all T_f studied in this work (including as-made samples), show the vast majority of the structural grains having a clear coarse modulation with wavelengths ranging from 35 to 45 nm. We see no appreciable changes of these periods with T_f. As shown in the TEM micrograph of Fig. 4(a), this coarse modulation is clearly seen as long stripes of light and dark contrast running across the whole grain. The observation of this contrast comes from both the slightly different absorption coefficients for each composition coupled to the difference in Co content between regions. This is clearly seen from the comparison of the *x*-ray microanalysis of these regions, in Fig. 4(b), indicating a spinodally decomposed grain.

Some words of warning to this respect are in order: the rather clear change in shading from one stripe to the next, seen in Fig. 4(a), is a combined result of the tilt and illumination conditions for local changes in Co concentration within the focused regions. These features, associated with the electron microscope settings, produce the clear-cut contrast in two shades and should not be considered as a proper sharp interface. The description of the real spatial distribution of Co should most likely be a smooth, continuous, almost sinusoidal function of the length in the anisotropy di-

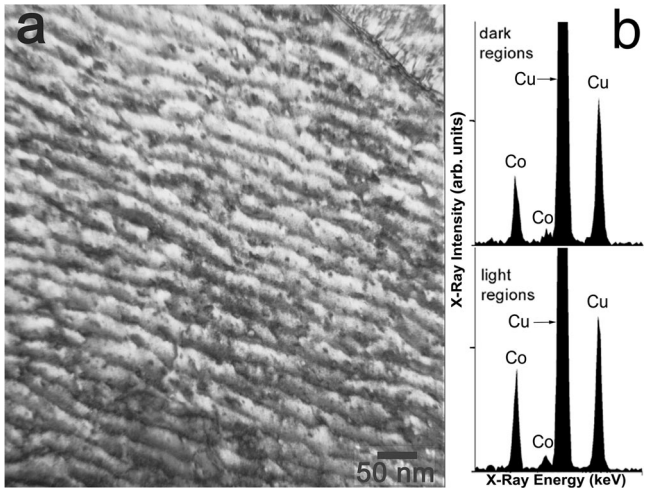

FIG. 4. (a) TEM micrograph showing a lamellar spinodal decomposition within a structural grain of a $Cu_{90}Co_{10}$ as-made sample. A clear coarse modulation of quasiperiodic stripes with wavelengths of 40 nm is observed; (b) *x*-ray microanalysis (EDS) from dark and light contrast regions of the lamellae of (a). Note the slight difference in Co content observed from the intensity of K_α lines of dark and light regions.

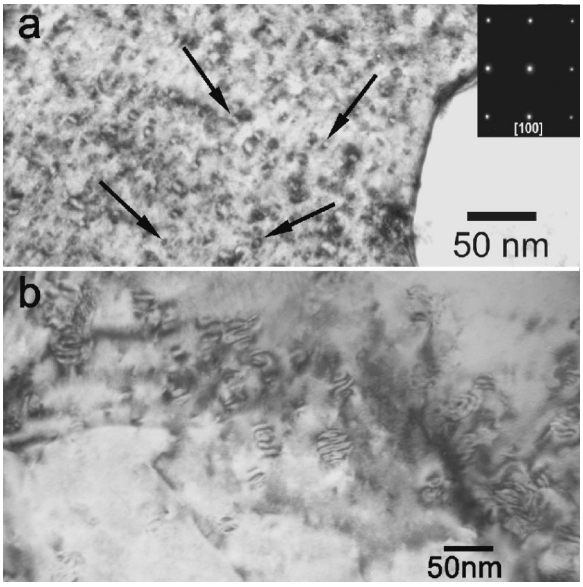

FIG. 5. Few dispersed precipitates are also seen in the samples: (a) Small coherent Co precipitates of ~5-nm size (seen as ringlike objects (Ref. 29), see pointing arrows), observed in an unannealed sample. They were observed under BFZA method along [100] axis zone. Inset: diffraction pattern at the [100] direction; (b) larger noncoherent Co precipitates of 30-nm size (seen as groups of interference fringes) concentrated along a dislocation region are observed in a sample annealed at $T_f = 873$ K. No lamellar is seen in these two cases.

rection. Real samples with defects, stresses, and the like may deviate from that ideal picture by slightly changing periods or directions of growth with respect to the theoretical prediction, but always keeping the smooth transition from one region to the next that characterizes this kind of segregation.

Albeit limited by the constraints of our microscope maximum possible tilt of the electron beam with respect to the sample, nearly 90% of the regions explored with TEM show this coarse lamellar modulation. A few grains in our samples failed, however, to exhibit the same modulated contrast, even when observed under different diffraction conditions. But the presence of some grains that did not undergo lamellar spinodal decomposition is expected in energetic terms, as the local temperature during the fast quench, or the local Co content in each grain, may have been thermodynamically unfavorable for the appearance of such a microstructure.

On account of our isochronal annealing procedure, we were able to observe the initial stages of the transformations induced by the anneals. In our work, we found no significant changes in the wavelength of the modulations of the stripes associated with different anneals, in apparent disagreement with the isothermal results of Busch *et al.*[17] We should say a few words about isochronous anneals, as most of the works published in this field are based on isothermal treatments. In our (isochronous) treatments, the temperature is swept continuously up to the final annealing temperature T_f. This implies that heat is transferred gradually to the sample, and the transformations depend on the heating rate. Isothermal anneals are easier to understand if one is speaking of very slow processes: the amount of heat is directly proportional to the time of the anneal, so the transformations are neatly proportional to time. However, the time that the sample takes to arrive at the annealing temperature is neglected in comparison to the total time. When isothermal annealing is used for aging, as it was the case in the work of Busch *et al.*,[17] the initial transformations are not observed for segregation, as these are rather fast phenomena. In fact, the amount of energy transferred to the sample is much smaller in isochronal anneals (where the temperature is raised steadily), as opposed to the isothermal treatments that deliver substantially larger total heat quantities, taking the system directly into the late stages of the transformations. Nevertheless, the initial stages may contain most of the relevant transformations in these samples and are the point of interest of our study. The results for the highest final annealing temperatures (or long annealing times) are expected to be equivalent for either isothermal or isochronous treatments with equivalent energy transfer,[28] for those systems where a final thermodynamic state can be defined. As we shall see below, our isochronous results show both the initial lamellar segregation (of 40 nm) and the latter one (4 nm), which would correspond to Busch *et al.*[17] late stage observations.

Along with the stripes, small coherent Co precipitates of few nanometers size (recognized by their ring-shape strain contrast[29]) also appear for all samples studied under Bright Field Zone Axis (BFZA) conditions.[15] These small precipitates (~5 nm) are homogeneously distributed over the grains and have no particular preference for grain boundaries, as seen in Fig. 5(a).

For higher annealing temperatures $T_f = 823$ and 873 K, a small number of grains also show larger noncoherent Co granules, around 30 nm size, as can be seen in Fig. 5(b). Those grains failed to show any contrast that could be associated with lamellar (spinodal) decomposition. These larger granules are seen preferentially in the regions of dislocation

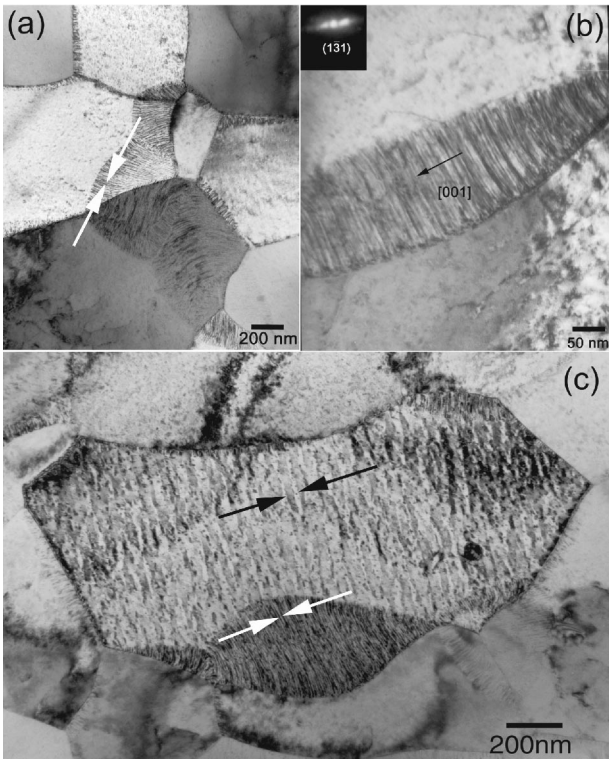

FIG. 6. A secondary lamellar decomposition is present in some samples after annealed at highest $T_f = 873$ K: (a) Grains showing heterogeneous small lamellar structures at the grain boundaries. Arrows indicate the modulation periods of the lamellae; (b) Enlarged portion of a grain boundary showing this finer decomposition of 4-nm narrow stripes running perpendicularly to the [001] directions of the cubic matrix. Inset: typical splitting of the diffraction pattern of spinodal decomposition (Ref. 19) for $(1\bar{3}1)$ reflection; (c) typical structural grain of $\approx 2000 \times 1000$ nm^2 fully segregated showing both types of lamellae, with large and small modulation periods, running along the same direction. Black and white arrows indicate for comparison the corresponding periods.

strain contrasts. In these regions, like those in Fig. 5(b), observation under BFZA contrast did not show any small Co precipitates, suggesting that the presence of the larger ones may be due to the growth of the smaller ones. We should mention that the appearance of Co precipitates of any size indicates, of course, that nucleation mechanisms and coarsening are acting simultaneously on the segregation process. This could probably be due to inhomogeneous heat transfer during the rapid quench, which is one of the key factors to induce nucleation.[19]

Remarkably, at the highest T_f (873 K), we found in some samples an additional decomposition in the form of narrow stripes with smaller period that develop heterogeneously, starting from the grain boundaries [see Fig. 6(a)] and running mostly along the [001] directions of the cubic matrix [Fig. 6(b)]. These formations display the typical splitting of the $(1\bar{3}1)$ reflection [see Fig. 6(b), inset], characteristic of spinodal alloys.[19] These finer lamellae were scarcely seen in other samples of lower T_f, although evidence of the initial stages of its formation was found in some $T_f = 823$ K samples. The direction of growth of these narrow lamellae is the same as that of the wide ones, as shown in Fig. 6(c), where both kinds of lamellar structures are seen in the same structural grain. This is a result of the elastic energy anisotropy inducing the composition profile to develop along certain preferred crystallographic directions.

C. Discussion

A description of these microstructures should be based on the thermal history of the samples. The large 40-nm periodic segregation must have been frozen-in during production, due to the very fast quenching rates for melt spinning, around 5×10^5 K/s. The narrower 4-nm lamellar formations seen for high T_f (where, coincidentally, MR decreases), growing at the grain boundaries would then correspond to a secondary process, occurring at a much slower cooling rate. This would be the case for the cooling down after thermal treatments (with quenching rates around 2.5 K/s). This is observed provided the samples are treated above $T_f = 823$ K, high enough to allow decomposition upon quenching according to the phase diagram,[13] but lower than the coexistence temperature for starting nucleation processes. The range of temperatures explored in the anneals (from 300 to 873 K) is characterized by huge changes in the atomic mobility, which is increased by a factor of 10^{24} with respect to room temperature,[14] therefore allowing for metastable and/or unstable segregation (''uphill diffusion'') processes to take place.

We have shown that $Cu_{90}Co_{10}$ melt-spun ribbons cannot be described as simple granulars where one would find small saturated Co superparamagnetic particles homogeneously dispersed in the copper matrix. For T_f above 823 K, as seen in Fig. 5, formation of large Co-rich precipitates is indeed observed in a small fraction of the grains that do not show any lamellar decomposition but, even if intergranular interactions and/or cluster size distributions are considered, it seems very unlikely that those few granules alone could produce such noticeable changes (increase by a factor of 2 and subsequent 35% reduction) of MR. We have, in turn, observed that the reduction of the MR is related to the appearance of the narrow stripes at the grain boundaries, identified as a secondary spinodal decomposition that forms in the irreversible region.

We believe the behavior of the resistivity during the anneals and the resulting magnetoresistance to be intimately connected to the microstructures of the ribbons. As stated by Kolometz and Smirnov, the residual resistivity in a spinodally decomposed region of a binary alloy changes as the variation of the amplitude of the concentration oscillations takes place.[30] That is, upon increasing the annealing time in isothermal anneals (or T_f in isochronal treatments), the amplitude of the oscillation increases, irrespective of the period for the lamellae, and this changes the residual resistivity. This also translates into increasing the MR, changing both the residual resistivity and its magnetic contribution (as long as the segregated Co is magnetic). The appearance of a second decomposition period would certainly have a swifter effect on the magnetoresistance mainly by inducing large changes on the magnetic component of the MR rather than from changes on the zero-field resistivity, as can be inferred from Fig. 3(d).

Apart from our TEM study, we have a further evidence for the description of these quasiperiodic Co-rich regions coming from magnetic force microscopy studies performed on the very same samples used for the TEM analysis presented here. Although still preliminary, the results[31] clearly show regions of magnetic orientation of approximately the same size and periodic nature observed for the nanoscopic lamellae in TEM micrographs. This requires a detailed description of the samples in terms of magnetic moment distributions compatible with the microstructures observed.

IV. CONCLUSIONS

We have measured *in situ* the resistivity of a series of melt-spun samples of nonequilibrium CuCo ribbons during specially designed isochronous anneals interrupted at different final treatment temperatures T_f and cooled immediately after. Each sample was thermally treated only once. We have also measured the magnetization and magnetoresistance as functions of applied field and temperature, as well as obtained TEM images and *x*-ray microanalysis to characterize the microstructures for each step of the annealing process.

We succeeded in establishing a relation between the nanoscopic structures and magnetotransport properties. The sizeable GMR seen, even for as-made CuCo samples, must be related to the large, homogeneous, lamellar spinodal decomposition in the form of parallel nanometric stripes (40 nm) appearing within the structural grains. This must be a result of the natural segregation that takes place during the melt-spinning process and strongly suggests that this kind of self-organized microstructure is indeed one of the possible configurations leading to GMR in these materials. Such a segregation might be incomplete for the fast quenching rates of melt spin, $\approx 5\times 10^5$ K/s, so we naturally expect that the subsequent isochronous anneals continue to develop the lamellar segregation by increasing the amplitude of the oscillations, thus enhancing MR, until the segregated (magnetic?) material is saturated. An irreversible region is found, starting at 650 K, above which the magnetization and MR are substantially enhanced while the resistivity decreases. Anneals beyond 823 K develop a secondary segregation with a smaller modulation period (4 nm), affecting substantially the magnetoresistance properties. We report that the only relevant microstructural changes we have seen, associated with the sudden decrease of MR in the high-temperature irreversible region, are the appearance of the finer nanostripes developing at the grain boundaries, most probably, a result of the second quench after annealing.

Our results thus demand a new rationale for the possible sources of spin-selective electronic scattering in these materials consistent with the nanoscopic scales imposed by these periodic stripes. This must consider, as we claim, the quasiperiodic microstructures reported in this work, having magnetic regions with inhomogeneous moment distributions that change in content with the thermal treatments. Such a scenario is quite different from the multilayer or pure granular cases and shows that the composition modulation can lead to giant magnetoresistance.

ACKNOWLEDGMENTS

We thank M. Knobel for providing us with the samples and M. A. Z. Vasconcellos for careful reading of the manuscript. One of us (E.E.R.) acknowledges partial support from Brazilian agencies CNPq and FAPERGS. We also acknowledge financial support from PRONEX/FINEP/CNPq (Brazil), under Contract No. 4196090700.

[1] M.N. Baibich, J.M. Broto, A. Fert, F. Nguyen Van Dau, F. Petroff, P. Etienne, G. Creuzet, A. Friederich, and J. Chazelas, Phys. Rev. Lett. **61**, 2472 (1988).

[2] G. Binasch, P. Grnberg, F. Saurenbach, and W. Zinn, Phys. Rev. B **39**, 4828 (1989).

[3] A.E. Berkowitz, J.R. Mitchell, M.J. Carey, A.P. Young, S. Zhang, F.E. Spada, F.T. Parker, A. Hütten, and G. Thomas, Phys. Rev. Lett. **68**, 3745 (1992); J.Q. Xiao, J.S. Jiang, and C.L. Chien, *ibid.* **68**, 3749 (1992); J. Wecker, R. von Helmolt, L. Schultz, and K. Samwer, Appl. Phys. Lett. **62**, 1985 (1993); B. Dieny, A. Chamberod, J.B. Genin, B. Rodmacq, S.R. Teixeira, S. Auffret, P. Gerard, O. Redon, J. Pierre, R. Ferrer, and B. Barbara, J. Magn. Magn. Mater. **126**, 433 (1993).

[4] L.F. Schelp, G. Tosin, M. Carara, M.N. Baibich, A.A. Gomes, and J.E. Schmidt, Appl. Phys. Lett. **61**, 1858 (1992); A.E. Berkowitz, J.R. Mitchell, M.J. Carey, A.P. Young, R. Rao, A. Starr, S. Zhang, F.E. Spada, F.T. Parker, A. Hütten, and G. Thomas, J. Appl. Phys. **73**, 5320 (1993); J.Q. Xiao, J.S. Jiang, and C.L. Chien, IEEE Trans. Magn. **29**, 2688 (1993); J.Q. Xiao, J.S. Jiang, and C.L. Chien, Phys. Rev. Lett. **68**, 3749 (1992).

[5] M. El-Hilo, K. O'Grady, and R.W. Chantrell, J. Appl. Phys. **76**, 6811 (1994); D. Altbir, J. d'Albuquerque e Castro, and P. Vargas, Phys. Rev. B **54**, 6823 (1996); D. Altbir, P. Vargas, J. d'Albuquerque e Castro, and U. Raff, *ibid.* **57**, 13 604 (1998).

[6] S. Zhang, Appl. Phys. Lett. **61**, 1855 (1992); S. Zhang and P.M. Levy, J. Appl. Phys. **73**, 5315 (1993); P.M. Levy, J. Magn. Magn. Mater. **140-144**, 485 (1995); C.L. Chien, Annu. Rev. Mater. Sci. **25**, 129 (1995); H.E. Camblong, S. Zhang, and P.M. Levy, J. Appl. Phys. **75**, 6906 (1994); E.F. Ferrari, F.C.S. da Silva, and M. Knobel, Phys. Rev. B **56**, 6086 (1997).

[7] M.N. Baibich, M.G.M. Miranda, G.J. Bracho Rodríguez, A.B. Antunes, H. Rakoto, N. Negre, M. Goiran, J.M. Broto, E.F. Ferrari, F.C.S. da Silva, and M. Knobel, J. Magn. Magn. Mater. **196-197**, 45 (1999).

[8] B.R. Pujada, E.H.C.P. Sinnecker, A.M. Rossi, and A.P. Guimarães, Phys. Rev. B **64**, 184419 (2001).

[9] D. Kechrakos and K.N. Trohidou, Phys. Rev. B **62**, 3941 (2000).

[10] J. Vergara and V. Madurga, J. Phys.: Condens. Matter **14**, 7513 (2002).

[11] P. Panissod, M. Malinowska, E. Jedryka, M. Wojcik, S. Nadolski, M. Knobel, and J.E. Schmidt, Phys. Rev. B **63**, 014408 (2001).

[12] A. López, F.J. Lázaro, M. Artigas, and A. Larrea, Phys. Rev. B **66**, 174413 (2002).

[13] M. Hansen, *Constitution of Binary Alloys*, (McGraw-Hill, New York, 1958).
[14] J.-M. Liu, Z.G. Liu, Z.C. Wu, and X.K. Meng, J. Mater. Sci. Lett. **13**, 1699 (1994); A. Hütten and G. Thomas, Ultramicroscopy **52**, 581 (1993).
[15] I.S. Servi and D. Turnbull, Acta Metall. **14**, 161 (1966); F.K. LeGoues and H.I. Aaronson, *ibid.* **32**, 1855 (1984); R. Hattenhauer and P. Haasen, Philos. Mag. A **68**, 1195 (1993), and references therein.
[16] S. Matsumura, M. Toyohara, and Y. Tomokiyo, Philos. Mag. A **62**, 653 (1990).
[17] R. Busch, F. Gärtner, C. Borchers, P. Haasen, and R. Bormann, Acta Mater. **44**, 2579 (1996).
[18] I.J. Kim and K. Fukamichi, Surf. Sci. Rep. **13**, 167 (1997); I.J. Kim, H. Takeda, J. Echigoya, N. Kataoka, K. Fukamichi, and Y. Shimada, Mater. Sci. Eng., A **217-218**, 363 (1996).
[19] R. Wagner and R. Kampmann, in *Materials Science and Technology, Vol. 5: Phase Transformations in Materials* (VCH, Weinheim, 1991), p. 213.
[20] L.H. Chen, S. Jin, T.H. Tiefel, S.H. Chang, M. Eibschutz, and R. Ramesh, Phys. Rev. B **49**, 9194 (1994).
[21] M.G.M. Miranda, A.B. Antunes, G.J. Bracho-Rodríguez, M.N. Baibich, E.F. Ferrari, F.C.S. da Silva, and M. Knobel, J. Magn. Magn. Mater. **185**, 331 (1998).
[22] M. Fin and M.N. Baibich, Rev. Fís. Aplic. e Instrum. **4**, 290 (1989).
[23] Quantum Design DC SQUID, model MPMS XL (5T), operated in the RSO mode.
[24] F.C.S. da Silva, M. Knobel, E.F. Ferrari, J.C. Denardin, M.G.M. Miranda, G.J.B. Rodríguez, A.B. Antunes, and M.N. Baibich, IEEE Trans. Magn. **36**, 3041 (2000).
[25] A.D.C. Viegas, J. Geshev, L.S. Dorneles, J.E. Schmidt, and M. Knobel, J. Appl. Phys. **82**, 3047 (1997).
[26] B.D. Cullity, *Introduction to Magnetic Materials* (Addison-Wesley, Reading, 1972).
[27] M.G.M. Miranda, A.B. Antunes, G.J. Bracho Rodríguez, and M.N. Baibich, J. Magn. Magn. Mater. **226-230**, 1638 (2001).
[28] M.A.Z. Vasconcellos, R.P. Livi, and M.N. Baibich, J. Phys. F: Met. Phys. **18**, 1343 (1988).
[29] R. Hattenhauer and F. Haider, Scr. Metall. Mater. **25**, 1173 (1991).
[30] I.D. Kolometz and A.A. Smirnov, Phys. Met. Metallogr. **14**, 1 (1962).
[31] M.G.M. Miranda, A. Morrone, G. Martínez, and M.N. Baibich (to be published).